Fusing of a Continuous Output PDR Algorithm With an Ultrasonic Positioning System

Vincent Thio, *Member, IEEE*, Joaquín Aparicio, *Member, IEEE*, Kjetil Bergh Ånonsen, Jan Kenneth Bekkeng, and Wilfred Booij

***Abstract*—The availability of inertial navigation sensors in smartphones has facilitated the development of pedestrian dead reckoning (PDR) models on a large scale. These models often consist of a step detection algorithm combined with a heading estimation routine. Common approaches to step detection include searching for peaks/valleys in the acceleration signal, principle frequency estimation, and machine learning techniques. Since the sensors embedded in smart devices are prone to noise, the position error grows unbounded if unchecked and requires periodical corrections based on external measurements. In this work, we propose a novel step detection algorithm based on sine-wave approximation of the acceleration signal. This method detects step fractions as well as full steps, which allows for continuous and real-time updates. The step detection algorithm is combined with a heading estimation routine described in our previous work to obtain a stand-alone PDR model. To mitigate error accumulation, we fuse the proposed model with position and heading measurements provided by a commercial indoor positioning system based on ultrasound. We evaluate the performance of the PDR and fused model in an open office environment, by walking along a trajectory while carrying a smartphone in hand or in the pocket. The results demonstrate the feasibility of the sine-wave approximation approach to step detection, as well as the expected benefits of fusing PDR with the ultrasonic system.**

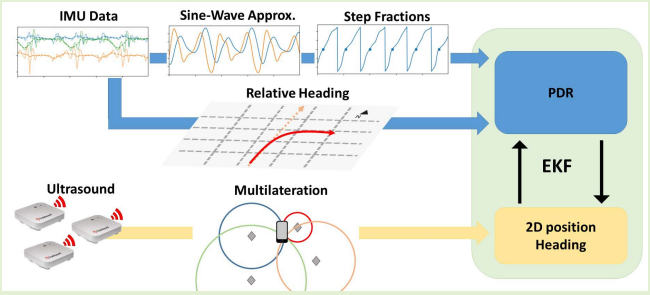

***Index Terms*—Indoor positioning, pedestrian dead reckoning, step detection, ultrasonic positioning system.**

I. Introduction

SMART devices have boosted the development of Location Based Services (LBS) in recent years, due to their diverse set of embedded sensors and widespread availability. LBS utilize the position of a device, often a smartphone or smartwatch, to provide location specific information and services. In outdoor and open areas, the position estimation process is typically based on a Global Navigation Satellite System (GNSS). In indoor environments, accurate positioning remains a challenge due to the high attenuation and distortion of GNSS signals when propagating through buildings. Due to the wide range of use cases, no consensus has yet been reached regarding a single, all-purpose Indoor Positioning System (IPS) for smart devices. Rather, many different types of IPS and related technologies have been developed over the last couple of decades.

Systems based on radio frequency (RF) signals are a popular choice [1], [2], due to the ubiquity of Wi-Fi access points in buildings. The accuracy of these systems is relatively low, typically in the order of a few meters [3]. Besides, radio waves penetrate relatively easily through building infrastructure, making it harder to distinguish between adjacent rooms or floors. This has a direct impact on user experience and limits the applicability of RF-based systems. A strong alternative to RF are ultrasonic signals. Contrary to radio waves, ultrasonic signals are largely contained within the room of the transmitter. Systems based on ultrasound can thus solve the adjacent room problem. The lower speed of sound also allows for much higher accuracies in terms of range estimates, in the order of centimeters [4]. Ultrasonic signals are, however, sensitive to multipath and Doppler effects [5], which can hinder the overall

Manuscript received September 10, 2021; revised November 19, 2021; accepted December 6, 2021. Date of publication December 9, 2021; date of current version January 31, 2022. This work was supported by the Research Council of Norway under Project 269614. The associate editor coordinating the review of this article and approving it for publication was Prof. You Li. *(Corresponding author: Vincent Thio.)*

Vincent Thio is with the Department of Physics, University of Oslo, 0371 Oslo, Norway (e-mail: vmthio@matnat.uio.no).

Joaquín Aparicio is with the Department of Informatics, University of Oslo, 0373 Oslo, Norway (e-mail: joaqapar@ifi.uio.no).

Kjetil Bergh Ånonsen is with the Norwegian Defence Research Establishment (FFI), 2027 Kjeller, Norway, and also with the Department of Technology Systems, University of Oslo, 0371 Oslo, Norway (e-mail: kjetil-bergh.anonsen@ffi.no).

Jan Kenneth Bekkeng is with the Norwegian Defence Research Establishment (FFI), 2027 Kjeller, Norway, and also with the Department of Physics, University of Oslo, 0371 Oslo, Norway (e-mail: j.k.bekkeng@fys.uio.no).

Wilfred Booij is with Forkbeard Technologies AS, 0283 Oslo, Norway (e-mail: wilfred.booij@forkbeardtech.com).

Digital Object Identifier 10.1109/JSEN.2021.3134468

performance of such a system. Both RF and ultrasonic systems have in common that they rely on some form of infrastructure, e.g., beacons or Wi-Fi access points. Even for optimized beacon distributions, there often remain some regions with low coverage and poor results, reducing the overall reliability of the system [4].

Inertial Navigation Systems (INS) provide positions without the need for a dedicated infrastructure. Instead, positions are based on dead reckoning, where information regarding device heading, speed, and time are integrated and subsequently added to the last known position. Historically, dead reckoning was mainly used in marine [6], air [7] and car navigation [8], especially before the introduction of GNSS. More recently, dead reckoning has expanded into the field of pedestrian navigation, in a process commonly referred to as Pedestrian Dead Reckoning (PDR) [9]–[13]. This expansion has, in large part, been facilitated by the global adoptation of smart devices containing the necessary sensors for inertial navigation. These sensors primarily include a 3-axis accelerometer and 3-axis gyroscope, combined in the Inertial Measurement Unit (IMU), and a 3-axis magnetometer.

PDR consists of a step or walk detection algorithm and some form of user heading estimation. The aim of a step detection algorithm is to provide a real-time estimate of accumulated steps or step fractions based on IMU measurements. A typical approach is to look for peaks, valleys or a combination thereof in the acceleration signal [14]–[17]. Other methods include principle frequency estimation [18]–[20] and feature extraction combined with machine learning techniques [21], [22]. Each method has its pros and cons, including sensitivity to false positives (e.g., false peak detections), computational intensity, requiring substantial historical data, and/or pre-training of the the algorithm. Given an estimated step length, the step detection algorithm provides an estimate of the distance travelled. This does not yet include the direction of travel, or heading. A common approach to inertial heading estimation is to compute the change in device attitude based on gyro data, sometimes complemented by the accelerometer and magnetometer [23]. A known device attitude allows for Principle Component Analysis (PCA) from which the direction of movement can be derived [24]. An alternative is to compute the gravity vector first, and apply it directly to the gyro measurement to extract the horizontal rotation [25], [26]. The latter method implicitly assumes that the change in horizontal orientation of the device is equal to the change in heading of the person carrying the device.

INS are subject to error accumulation due to sensor noise and limitations of the applied model. In the specific case of PDR, main error sources include residual gyro bias and bias drift, causing attitude drift over time, unresolved variations in step length, and incorrect classification of detected steps. Error accumulation requires periodical corrections based on an external system. Therefore, PDR is often fused with an infrastructure-based positioning system, typically in a Kalman filter setup. A fused system exploits the best of both worlds: high-accuracy IPS measurements correct position deviations generated by the PDR model, whereas the continuous availability of PDR mitigates areas poorly covered by the IPS. In this work, we will use an Ultrasonic Indoor Positioning System (UIPS) to generate external measurements.

Several examples of fused systems based on inertial measurements and ultrasonic signals can be found in literature. In [27], ultrasonic beacons were deployed in the ceiling, and three receivers were carried by a robot. Time-Of-Flight (TOF) measurements were fused with odometry information to obtain the required input for the correction phase of the Kalman filter. The prediction phase consisted of odometry readings alone. The system in [28] was able to detect Non-Line-Of-Sight (NLOS) conditions using a classifier. If that situation occurred, an INS provided a position estimate based on the step count derived from accelerometer data, and heading based on the compass. These inertial measurements were inputs to the propagation phase of an Extended Kalman Filter (EKF). For the measurement model, the last estimated position from TOF measurements was used. In [29], a smartphone acted as the ultrasonic transmitter, and a network of beacons as receivers. Position was calculated in a central unit. In case of no coverage by the ultrasonic system, the inertial sensors from the smartphone provided the position, calculated from the step length and orientation. This ultrasonic system was later used in [30] to fix the position estimates provided by an INS based on a Fuzzy Inference System (FIS). FIS was used to reduce the error in velocity and position after integration, caused by the remaining gravity component. Both positions were fused in a Kalman filter. One of the most recent examples was described in [31]. Several ultrasonic modules, each containing five beacons, were deployed at key points in the test area. To enable navigation in areas with limited ultrasonic coverage, an external INS was attached to the user's leg, and connected to the device via Bluetooth. It calculated the step length from the pitch signal, obtained from an EKF. Together with the rotation angles it provided position and orientation. This information was fused with the ultrasonic positions in a second EKF.

In this work, we present a novel step detection algorithm based on sine-wave approximation of the accelerometer signal. The proposed algorithm does not require significant fine-tuning or historical data to function, although historical data may be used in addition to improve its robustness. The step detection algorithm is combined with a heading estimation method, developed previously by the authors [26], to obtain a stand-alone PDR algorithm. This PDR algorithm is fused with positions and heading measurements obtained from a UIPS. The fusion process is based on an EKF setup. We test the PDR and fused methods in two scenarios: 1) a phone in the hand, and 2) a phone in the pocket, while walking through an open office environment with significant NLOS conditions.

The rest of the paper is organized as follows: Section II describes the step detection algorithm, the inertial heading estimation process, and the dynamic model of the PDR algorithm. An overview of the UIPS is given in Section III. The EKF setup is described in Section IV. We present the experimental setup and results in Section V, with conclusions in Section VI.

II. Pedestrian Dead Reckoning

This section describes the main components of the inertial navigation process. First, we introduce a novel step detection algorithm based on sine-wave approximation of accelerometer data. This is followed by a description of the inertial heading estimation process, and finally the dynamic model, which combines the two into a stand-alone PDR algorithm.

A. Step Detection Algorithm

The 3-axis accelerometer measures the specific force, denoted $\boldsymbol{f}$, as the sum of the instantaneous user acceleration and local gravity. The first step is to apply a low-pass filter to each of the three axes of the accelerometer to reduce the effect of sensor noise and small movements unrelated to the walking motion. In this study, we use a second-order Butterworth filter with a cut-off frequency at 2.5 Hz, based on the upper limit of typical walking frequencies [32].

The filtered signal is used to calculate the gravity-free acceleration norm, denoted a, by computing the Euclidean norm and removing the local gravity magnitude:

$$a(t) = \sqrt{f_x(t)^2 + f_y(t)^2 + f_z(t)^2} - g, \tag{1}$$

where f_i, with $i = x, y, z$, denotes the filtered accelerometer signal, and g the local gravity magnitude. The walking motion is a recurrent process, so the corresponding gravity-free acceleration norm signal constitutes a periodical function. Typical pedestrian acceleration profiles show that this periodical function can be approximated by a sine wave,

$$a(t) \approx A \sin(2\pi f_w t), \tag{2}$$

where f_w is the walking frequency and A an unknown amplitude. In addition, we define the scaled derivative of the above equation as

$$\dot{a}^*(t) \approx A \cos(2\pi f_w t), \tag{3}$$

where a scaling factor $(2\pi f_w)^{-1}$ has been applied to ensure that the amplitudes are equal in both functions. The gravity-free acceleration norm and its derivative can be represented by a complex number, where the real part is given by $a(t)$ and the imaginary part by $\dot{a}^*(t)$. Given a discrete accelerometer measurement $\boldsymbol{a}_k = \boldsymbol{a}(t_k)$, we can now compute a "step completeness" estimate ϕ_k^c based on the phase angle,

$$\phi_k^c \approx \frac{1}{2\pi} \operatorname{atan2}\left(\dot{a}_k^*, a_k\right), \tag{4}$$

where the $(2\pi)^{-1}$ scaling factor ensures that the value of ϕ_k^c falls within the interval $[-0.5, 0.5]$. The step completeness estimate represents the current step fraction based on a single step. Thus, a value close to -0.5 indicates the start of a step, whereas a value close to $+0.5$ indicates the end of a step. The total fractional step count, ϕ_k, keeps track of the total number of steps taken by the pedestrian. This value gets updated for each incoming step completeness estimate according to

$$\phi_{k+1} = \phi_k^c - [\phi_k^c - \phi_k], \tag{5}$$

where the brackets indicate rounding to nearest integer and $\phi_0 = -0.5$. To filter out small movements unrelated to the walking motion, (4) is only evaluated if the magnitude of the complex number described by a and $\dot{a}^*$ exceeds a predefined threshold. Otherwise, the measurement is rejected and $\phi_{k+1} = \phi_k$. The threshold value was determined empirically for a phone in hand and a phone in pocket, and set to 0.02 g for all experiments presented in this work. Fig. 1 shows the results of an implementation of the step detection algorithm for a phone carried in the pocket. The individual steps are difficult to extract from the raw (solid lines) and smoothed (dashed lines) accelerometer data (top), but become more apparent in the gravity-free acceleration norm plot (middle). The step completeness plot (bottom), however, gives a much clearer representation of the continuous trend of individual steps. The proposed algorithm provides step fractions, in addition to full steps, which allows for continuous and real-time updates. This in contrast to conventional algorithms using peak/valley detection, which typically provide updates at discrete intervals, based on the detection of full steps.

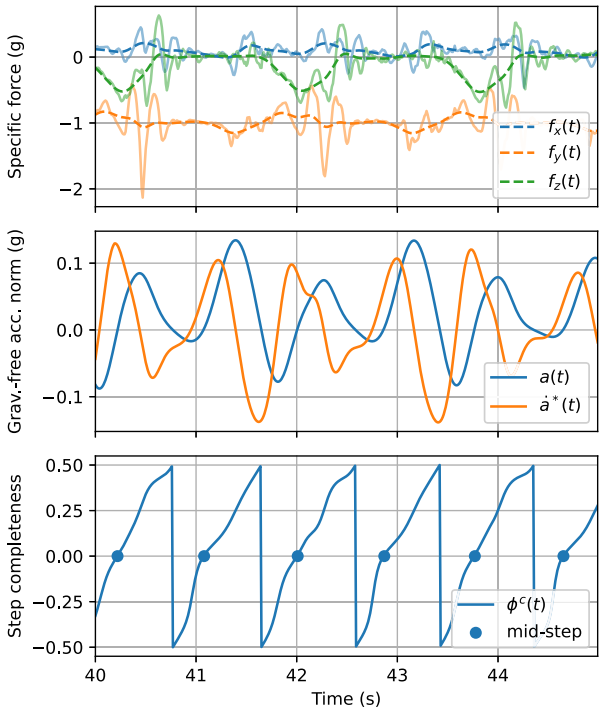

Fig. 1. Step detection algorithm example. Top: raw (solid) and smoothed (dashed) accelerometer data. Middle: gravity-free acceleration norm and its scaled derivative. Bottom: the phase angle, scaled down to a $[-0.5, 0.5]$ range, shows the completeness of individual steps. A clear continuous trend is shown for each step.

Eq. (4) and (5) are based on a single acceleration measurement and therefore sensitive to temporal perturbations of the user acceleration, as well as artifacts related to the underlying sine-wave approximation. The robustness of the algorithm can be improved by adding a simple linear regression over the last N estimates. This alternative process requires N samples for it to be initialized, but still provides output in real time for subsequent estimates. Setting $i = k - N$, and defining the vectors $\boldsymbol{\phi} = [\phi_i, \ldots, \phi_k]$ and $\boldsymbol{t} = [t_i, \ldots, t_k]$, the fitting parameters of the linear expression $\phi(t) = A + Bt$

are given by (6),

$$A = \phi_{av} - B t_{av}$$
$$B = \frac{\sum_{i=1}^{N} (t_i - t_{av})(\phi_i - \phi_{av})}{\sum_{i=1}^{N} (t_i - t_{av})^2} \tag{6}$$

where ϕ_{av} and t_{av} are the vector averages, and the gradient B provides a new estimate of the walking frequency. The linear fit is accepted if B falls within the expected walking frequency range, $f_{w_{min}} < B < f_{w_{max}}$, with $f_{w_{min}} = 0.5$ Hz and $f_{w_{max}} = 2.5$ Hz. The new walking frequency can be used as input to (2) and (3) of the next iteration. The new "best estimate" of the total fractional step count becomes,

$$\overline{\phi}_k = A + B t_k. \tag{7}$$

This value is used in the propagation phase of the EKF to compute displacement between IMU measurements.

B. Relative Heading Estimation

The inertial heading estimation process applied here provides the change in user heading, $\Delta\psi$, based on IMU measurements. This process builds upon the assumption that the change in user heading is equal to the change in horizontal orientation of the device, also known as yaw. This assumption is generally valid if the device position with respect to the carrier remains constant, e.g., a phone in the pocket or a smartwatch attached to the wrist. The full derivation of the heading estimation algorithm, developed by the authors in a previous work, can be found in [26]. The main components are summarized here.

Computing $\Delta\psi$ requires the horizontal component of the rotation rate, which can be extracted from a raw gyro measurement by way of the gravity vector. The gravity vector, denoted $\boldsymbol{\gamma}$, is a unit vector representing the "down" direction of the device in the local North-East-Down (NED) frame. Given a gyro measurement $\overline{\boldsymbol{\omega}}_k$ and estimated gravity vector $\overline{\boldsymbol{\gamma}}_k$, the change in yaw can be computed by forward integration,

$$\Delta\overline{\psi}_k = \overline{\boldsymbol{\omega}}_k^T \overline{\boldsymbol{\gamma}}_k \Delta t, \tag{8}$$

where Δt is equal to the inverse of the IMU rate. There are two main error sources contributing to the error of $\Delta\psi_k$. The first relates to sensor noise, and the second to errors contained within the gravity vector estimate. A first order approximation of the estimated error of $\Delta\psi_k$, described in terms of the variance $\sigma^2_{\Delta\psi_k}$, is given by

$$\sigma^2_{\Delta\psi_k} = \overline{\boldsymbol{\gamma}}_k^T Q \overline{\boldsymbol{\gamma}}_k + \overline{\boldsymbol{\omega}}_k^T P_{\gamma_k} \overline{\boldsymbol{\omega}}_k \tag{9}$$

where Q is the covariance matrix of the integrated gyro noise and P_{γ_k} the gravity vector covariance matrix. Assuming uncorrelated noise, Q is a 3-by-3 diagonal matrix whose elements are given by the variances of the individual sensor axes, multiplied by Δt^2. The propagation of P_{γ_k} is derived below and formalized in (13).

The heading estimation process requires the gravity vector to be known at all times. Given an initial vector $\overline{\boldsymbol{\gamma}}_0$ and associated covariance matrix P_{γ_0}, the gravity vector can be estimated by adjusting for device rotation. The change in device orientation is given by the rotation matrix R, which we obtain by forward integration of the rotation rate. Given a gyro measurement $\overline{\boldsymbol{\omega}}_k$, the rotation between t_k and t_{k+1} is given by,

$$R(\overline{\boldsymbol{\omega}}_k) = I + \sin(\alpha)\,[\boldsymbol{u}]_\times + (1 - \cos(\phi))\,[\boldsymbol{u}]_\times^2) \tag{10}$$

where $[\boldsymbol{u}]_\times$ is the skew-symmetric matrix of $\boldsymbol{u}$ and

$$\alpha = \|\overline{\boldsymbol{\omega}}_k\| \Delta t,$$
$$\boldsymbol{u} = \frac{\overline{\boldsymbol{\omega}}_k}{\|\overline{\boldsymbol{\omega}}_k\|}. \tag{11}$$

Applying $R_k = R(\overline{\boldsymbol{\omega}}_k)$ to the previous estimate of the gravity vector yields an updated estimate,

$$\overline{\boldsymbol{\gamma}}_{k+1} = R_k \overline{\boldsymbol{\gamma}}_k. \tag{12}$$

The corresponding gravity vector covariance matrix also requires the rotation matrix, plus an additional term to account for gyro noise. The time update of the gravity vector covariance matrix becomes,

$$P_{\gamma_{k+1}} = R_k P_{\gamma_k} R_k^T + [\overline{\boldsymbol{\gamma}}_k]_\times Q [\overline{\boldsymbol{\gamma}}_k]_\times^T. \tag{13}$$

The initial gravity vector estimate, as well as independent periodical corrections, are based on the accelerometer, e.g., by averaging the measured specific force over a period of time during which the device remains static.

C. State Vector and Dynamic Model

Combining the step detection algorithm with the inertial heading estimation process, we can now formalize the PDR model. This model consists of a state vector, describing the current state of the device/user, and a dynamic model, describing the change in state based on incoming IMU measurements. The state vector, denoted $\boldsymbol{x}$, is defined as follows,

$$\boldsymbol{x} = \begin{bmatrix} x & y & \psi & \boldsymbol{\gamma}^T \end{bmatrix}^T, \tag{14}$$

where (x, y) is the 2D position of the device, ψ the user heading, and $\boldsymbol{\gamma}$ the gravity vector. Since IMU measurements come in at discrete time intervals, the propagation of the state constitutes a discrete, non-linear estimation problem of the form

$$\boldsymbol{x}_{k+1} = f(\boldsymbol{x}_k, \boldsymbol{\omega}_k, \boldsymbol{f}_k, \Delta t), \tag{15}$$

where the dynamic model f is a function of the current state $\boldsymbol{x}_k$, the rotation rate $\boldsymbol{\omega}_k$, the specific force $\boldsymbol{f}_k$, and time increment Δt. The rotation rate is processed directly by the dynamic model according to (8)–(13), whereas the specific force is processed separately by the step detection algorithm. The latter produces the step increment $\Delta\phi_k = \phi_{k+1} - \phi_k$, and corresponding change in 2D position as,

$$\Delta x_k = \Delta\phi_k L \cos(\psi_k)$$
$$\Delta y_k = \Delta\phi_k L \sin(\psi_k), \tag{16}$$

where L is the step length. Since the step length may vary between steps, we assume that each step increment adds an independent amount of noise to the system. Therefore, the step length is not part of the state vector itself. Instead, step length variations will be introduced as uncorrelated noise, similar to

sensor noise. By combining (8), (12) and (16), we obtain the discrete dynamic model for PDR as

$$f(\boldsymbol{x}_k, \boldsymbol{\omega}_k, \boldsymbol{f}_k, \Delta t) = \begin{bmatrix} x_k \\ y_k \\ \psi_k \\ 0 \end{bmatrix} + \begin{bmatrix} \Delta\phi_k L \cos(\psi_k) \\ \Delta\phi_k L \sin(\psi_k) \\ \boldsymbol{\omega}_k^T \boldsymbol{\gamma}_k \Delta t \\ R(\boldsymbol{\omega}_k \Delta t)\boldsymbol{\gamma}_k \end{bmatrix}. \quad (17)$$

III. Ultrasonic Positioning System

In this section, we give a short summary of the UIPS used in this study to correct the PDR error. A detailed description and performance evaluation is given in [33]. This system, developed by Forkbeard Technologies AS [34], provides measurements of device position and velocity using an app on an iOS or Android smartphone. These measurements will be used for periodical corrections of the state vector. The UIPS is based on an infrastructure of battery-powered beacons with Bluetooth Low Energy (BLE) and ultrasonic capabilities. The system assigns a locally unique signature and time slot to each beacon. The beacons transmit their respective signatures periodically using a frequency modulated ultrasonic signal.

The receiving device, a smartphone, calculates the beacon range based on estimated TOF and Doppler derived radial velocity. In addition, it uses a buffer of historical Doppler derived velocities to extrapolate the last N range estimates, calculated at times $t_N \ldots t_1$, towards the current time t_0. Taking the weighted average yields the "Doppler stabilized range" for each beacon at t_0.

A 2D position estimate, $\boldsymbol{p}$, is generated for each valid incoming signature by optimizing the set of most recent Doppler stabilized beacon ranges. The algorithm also provides an estimation of the position error, based on the residual of the optimization routine. Assuming no correlation between errors, the position error is described by a covariance matrix P_p where all non-diagonal elements are equal to zero.

A 2D velocity vector $\boldsymbol{v}$ and corresponding covariance matrix P_v are computed in a similar fashion by optimizing the set of Doppler-derived radial velocities. The velocity vector is related to the user heading ψ as follows,

$$\psi = \cos^{-1}\left(\frac{v_x}{\|\boldsymbol{v}\|}\right) \quad (18)$$

where substituting $\boldsymbol{v} = \overline{\boldsymbol{v}}$, the computed value, gives the estimated user heading $\overline{\psi}$ in the local frame of the UIPS. The heading variance, σ_ψ^2, can be derived from (18) using a first order Taylor expansion and applying the product rule, giving

$$\sigma_\psi^2 = (1 - \overline{\psi})^{-1} M P_v M^T \quad (19)$$

where P_v again is the velocity vector covariance matrix, and the Jacobian M is given by

$$M = \frac{1}{\|\overline{\boldsymbol{v}}\|}\begin{bmatrix} \left(1 - \frac{\overline{v}_x}{\|\overline{\boldsymbol{v}}\|^2}\right) & \frac{\overline{v}_y}{\|\overline{\boldsymbol{v}}\|^2} \end{bmatrix} \quad (20)$$

The position ($\boldsymbol{p}$), heading (ψ) and corresponding error estimates (P_p and σ_ψ^2), generated by the UIPS are used in the correction phase of the EKF setup, described next.

IV. Fusing PDR With Ultrasonic Positions

Here, we describe the setup of the EKF which fuses the PDR output with measurements from the UIPS. The EKF consists of three distinct phases: the initialization phase, the propagation phase and the correction phase. The initialization phase is based on both IMU and ultrasound data, the propagation phase on IMU data alone, and the correction phase on ultrasound data.

A. Initialization Phase

The filter requires a 2D position, heading, gravity vector and step length for initialization. The initial gravity vector is derived from accelerometer data under static conditions, and should be determined before the initial position and heading are set. Therefore, the initial position and heading are based on the first valid ultrasonic measurement after initialization of the gravity vector. The step length, which typically varies between 0.5 and 1 m, is set to 0.7 m. We assume uncorrelated errors for the initial state, except for 1) the 2D position, and 2) the three components of the gravity vector. The initial state vector and associated covariance matrix become

$$\overline{\boldsymbol{x}}_0 = \begin{bmatrix} \overline{x}_0 \\ \overline{y}_0 \\ \overline{\psi}_0 \\ \overline{\boldsymbol{\gamma}}_0 \end{bmatrix}, \quad \overline{P}_0 = \begin{bmatrix} P_{p_0} & \cdots & \mathbf{0} \\ \vdots & \sigma_{\psi_0}^2 & \vdots \\ \mathbf{0} & \cdots & P_{\gamma_0} \end{bmatrix} \quad (21)$$

where σ_{ψ_0} is the standard deviation of the initial user heading, P_{p_0} is the 2-by-2 covariance matrix of the initial position, and P_{γ_0} the 3-by-3 covariance matrix of the initial gravity vector.

B. Propagation Phase

The EKF updates at discrete intervals, based on the measurement rate of the IMU. The estimated state follows directly from (15) by setting $\boldsymbol{x}_k = \overline{\boldsymbol{x}}_k$. The propagation of the covariance matrix requires the Jacobian of the dynamic model, given by (17), evaluated at $\overline{\boldsymbol{x}}_k$. The time-dependent Jacobian F_k becomes,

$$F_k = \begin{bmatrix} 1 & 0 & -\Delta\overline{y}_k & \mathbf{0}^T \\ 0 & 1 & \Delta\overline{x}_k & \mathbf{0}^T \\ 0 & 0 & 1 & \overline{\boldsymbol{\omega}}_k^T \Delta t \\ \mathbf{0} & \mathbf{0} & \mathbf{0} & R(\overline{\boldsymbol{\omega}}_k \Delta t) \end{bmatrix} \quad (22)$$

Variations in step length introduce additional errors into the 2D position estimate. Since these errors are generally uncorrelated, step length variations are modeled as additive white Gaussian noise, similar to sensor noise. The noise term containing the gyro sensor noise Q is thus extended to

$$Q^* = \begin{bmatrix} \sigma_L^2 & \mathbf{0} \\ \mathbf{0} & Q \end{bmatrix}, \quad (23)$$

where σ_L^2 is the step length variance. The noise term is related to the state vector by (9), (13) and (16), which together make up the G matrix,

$$G_k = \begin{bmatrix} \Delta\overline{x}_k / L_k & \mathbf{0}^T \\ \Delta\overline{y}_k / L_k & \mathbf{0}^T \\ \mathbf{0} & \overline{\boldsymbol{\gamma}}_k^T \\ \mathbf{0} & [\overline{\boldsymbol{\gamma}}_k]_\times \end{bmatrix}. \quad (24)$$

Combining (22)–(24), we now obtain a formulation of the propagation of the covariance matrix as

$$\overline{P}_{k+1} = F_k \overline{P}_k F_k^T + G_k Q^* G_k^T \tag{25}$$

C. Correction Phase

Corrections to the state vector are based on position and heading measurements generated by the ultrasonic system. The standard Kalman equations apply with $H = I_6$,

$$\begin{aligned} K_k &= \overline{P}_k(\overline{P}_k + P_k^z)^{-1} \\ \hat{\boldsymbol{x}}_k &= \overline{\boldsymbol{x}}_k + K_k(\boldsymbol{z}_k - \overline{\boldsymbol{x}}_k) \\ \hat{P}_k &= (I_6 - K_k)\overline{P}_k \end{aligned} \tag{26}$$

where $\hat{x}_k$ and $\hat{P}_k$ are the corrected state and covariance matrix, $z_k = [x_k, y_k, \psi_k, \boldsymbol{\gamma_k}^T]^T$ contains the ultrasound-based position and heading measurements (and gravity vector, if available), and P_k^z the corresponding covariance matrix. Since the UIPS does not provide gravity vector measurements, corrections to the gravity vector are independent from position and heading corrections. Instead, the gravity vector is corrected based on IMU data. See [26] for details.

V. Experiments and Results

This section describes the experiments we conducted to demonstrate the feasibility of the proposed PDR algorithm, both as a stand-alone system, as well as fused with external position and heading measurements.

A. Experimental Setup

The experimental data presented here were taken as part of a characterization study of the UIPS, see [33]. Data were collected using a Samsung Galaxy S9 smartphone, which was carried by a user while following a predefined walking trajectory at an average walking speed of 0.8 m/s. The IMU measurement rate was set to 100 Hz. The test area was approximately 150 m^2 and included furniture and panels to induce multipath and NLOS conditions. The test area was equipped with a Motion Capture (MoCap) system which provided a ground truth reference of the walking trajectory. The UIPS consisted of 10 beacons which provided position and heading measurements at an average rate of 10 Hz. An overview of the test area is shown in Fig. 2, with the walking trajectory marked in light-grey color.

The experiments consist of three parts. First, we test the accuracy of the step detection algorithm by comparing the total number of detected steps with the true number of steps. This is done by walking along a circular trajectory of approximately 50 steps. In the second part we test the fusion algorithm in two stages: first, we validate the fusion process by combining simulated PDR data with synthetic external measurements. The simulated PDR data are generated following the same update rate as the real PDR data (100 Hz) by converting MoCap positions into step increments and horizontal rotation increments. No artificial noise is added to the simulated PDR data. The synthetic external measurements are generated every second and derived from MoCap positions by adding Gaussian noise, described by standard deviation σ_p (m) for position and σ_h (deg) for heading measurements. In the second stage, we exchange the simulated PDR data for real data based on IMU measurements, while keeping the external measurements synthetic. This allows us to evaluate the performance of the PDR and fusion algorithms without the added uncertainties introduced by a real UIPS. In the third set of experiments, we use an actual UIPS to obtain real position and heading measurements. This allows us to assess the performance of the fusion algorithm under realistic conditions. Two UIPS setups are considered here: 1) a 10-beacon system with an update rate of 10 Hz, and 2) a reduced system of five beacons with an update rate of 1 Hz.

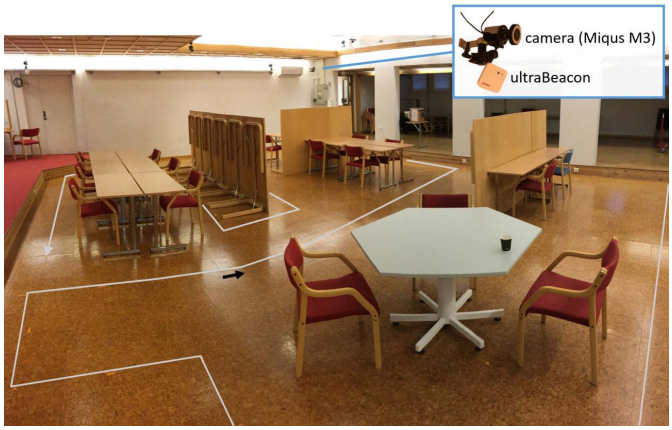

Fig. 2. Overview of the test area with "open office" setup, from [33]. Light-grey line indicates walking trajectory.

For all experiments, we focus on two phone positions: the first is a phone carried in the hand, at a fixed position in front of the carrier. This simulates navigation, in contrast to, for example, a "swinging hand" position. The second position is a phone carried in the left pocket. All IMU and ultrasonic data collected by the phone were processed offline.

B. Results

1) Experiment I: We performed two experiments, one per phone position, to test the accuracy of the step detection algorithm. For a phone carried in the hand, the algorithm counted a total of 55.4 steps over a trajectory of 54 true steps, yielding an accuracy of 97.5%. The accuracy increased to 99.9% for a phone carried in the pocket, based on 52.1 detected steps against 52 true steps. In both cases, the step detection algorithm detected more steps than the actual number of steps. This was due to false-positives at the end of the walking trajectory, where the user stopped walking but the phone still experienced some form of motion (e.g., moving the phone out of the carrying position).

2) Experiment II: The validity of the fusion algorithm was tested by performing three experiments using simulated PDR data. Each experiment involved fusion between PDR and synthetic external measurements at different noise levels. The results are shown by increasing levels of artificial noise as blue, orange and green lines in Fig. 3. All trajectories start in the top-right corner and initially show significant errors before converging towards the ground truth (grey line). Figure 4

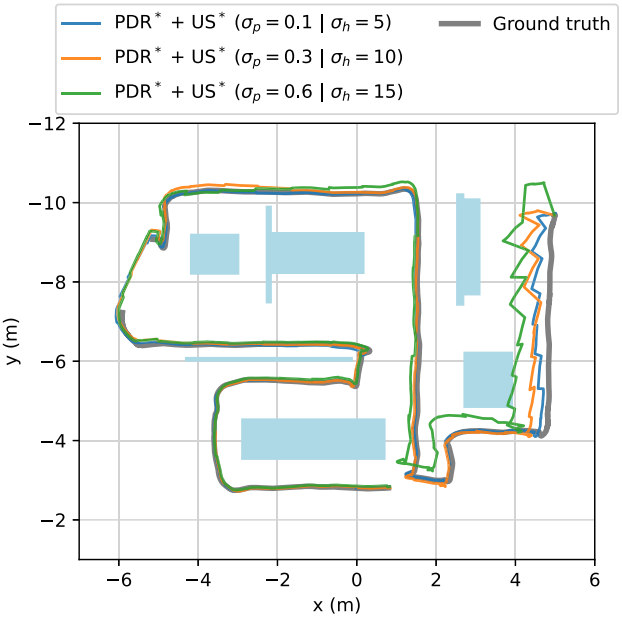

Fig. 3. Validation of the fusion algorithm: combining simulated PDR data with synthetic ultrasonic measurements. The PDR data (PDR*) was derived from the ground truth trajectory (grey line) and consists of step increments and horizontal rotation rates. Synthetic ultrasonic measurements (US*) were also based on ground truth and generated every second. The measurements contain artificial Gaussian noise with a standard deviation of σ_p (m) for 2D position and σ_h (deg) for heading. The PDR trajectory is not shown here, as it is very close to ground truth. The fused solutions with synthetic PDR and ultrasonic measurements are shown in blue, orange and green. The blue shapes represent the tables and obstacles of the "open office" setup, shown in Fig. 2.

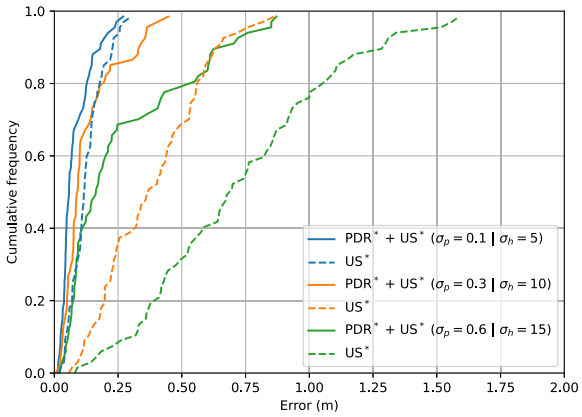

Fig. 4. CDF of the 2D position errors for the trajectories shown in Fig. 3. Dashed lines represent the errors of the synthetic 2D positions generated per trajectory. The solid lines represent the position errors produced by the fusion algorithm. As expected, the fused solution produces better results than the independent position measurements. Note that this involves 'ideal' circumstances, where the errors of the ultrasonic position measurements follow a Gaussian distribution and errors do not accumulate in the PDR algorithm.

shows the Cumulative Distribution Function (CDF) of the position error derived from the results. The dashed lines are based on the artificially generated 2D position measurements, and the solid lines on the 2D position of the fused solution taken at the same time instances. As shown, the fused solution always performs better than the independent synthetic position measurements. This is as expected and validates the

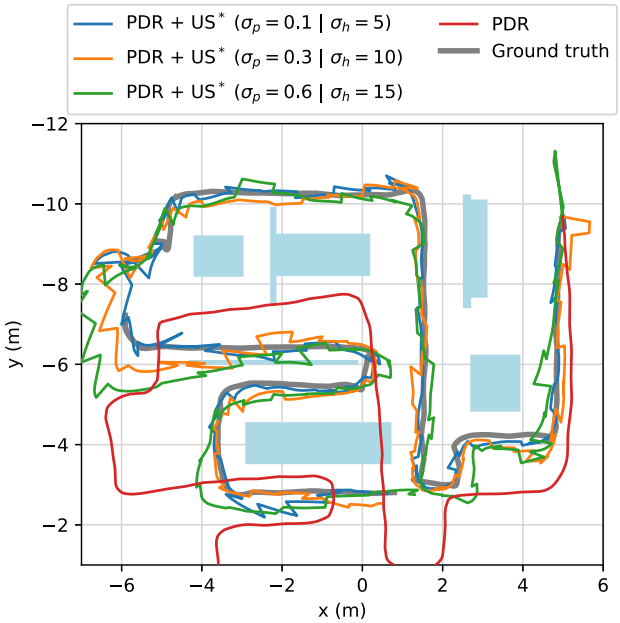

Fig. 5. Phone carried in hand, PDR fused with synthetic measurements. The PDR-based trajectory is shown in red, and the fused solutions with synthetic measurements (US*) are shown in blue, orange and green. The PDR algorithm detected a total of 84.1 steps.

theoretical base of the fusion algorithm. Next, we repeated the experiments by introducing real PDR data derived from a phone carried in hand and a phone carried in the pocket. Both cases contain an additional experiment based on PDR only (no fusion) for comparison. The results are shown in Fig. 5 for a phone carried in hand, and in Fig. 6 for a phone carried in pocket. The figures clearly demonstrate that a trajectory based on PDR alone, as shown in red, can divert quickly from its true trajectory. This is a common issue, since there are no further reference points after initialization and errors caused by step length variations, gyro drift, and unintended phone movements start to accumulate. The fusion-based experiments, on the other hand, are much closer to the ground truth trajectory.

Figures 7 (hand) and 8 (pocket) present the corresponding CDF of the 2D position errors for all fusion experiments. Both figures show the increasing value of PDR as the accuracy of the external measurements decreases. PDR does appear to have a negative effect for highly accurate external measurements, as shown by the blue-colored lines. This discrepancy between the simulated and real PDR experiments may indicate that the PDR algorithm produces residual non-Gaussian noise which cannot be resolved by the fusion process. Note, however, that PDR produces near-continuous position updates, whereas the external measurements are generated every second.

3) Experiment III: The final set of experiments focuses on fusing the PDR solution with real position and heading measurements obtained from two different UIPS setups. The results for the first setup, a 10-beacon configuration with a 10 Hz update rate, are shown in Fig. 9 for a phone carried in the hand, and in Fig. 10 for a phone carried in the pocket. Both figures show the independent position estimates generated by the UIPS as red dots, the estimated walking trajectory based on

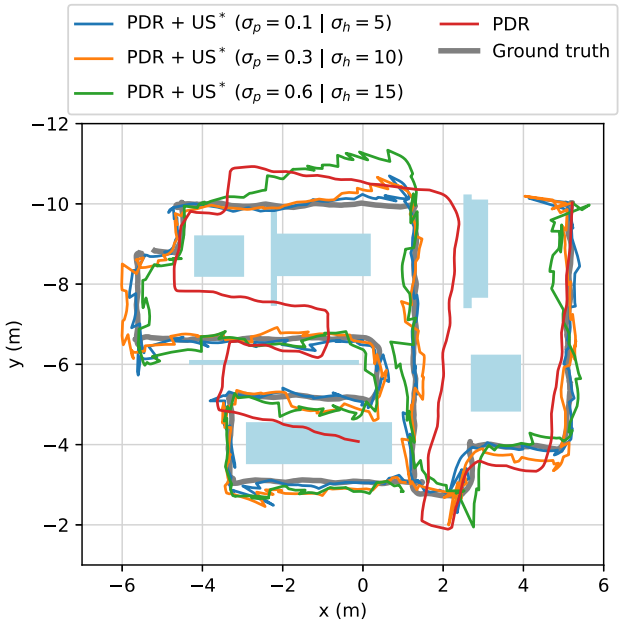

Fig. 6. Phone carried in pocket, PDR fused with synthetic measurements. PDR and fused (PDR + US*) trajectories are shown in red, blue, orange and green. Ground truth trajectory is given by the grey line. Fused trajectories are characterized by noise levels (based on σ_p for 2D position and σ_h for heading) and generated every second. 82.9 steps were detected by the PDR algorithm.

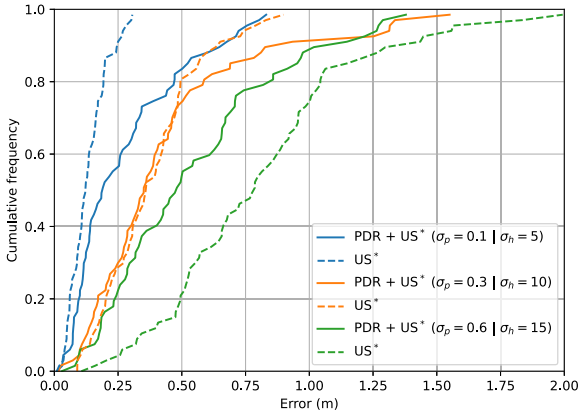

Fig. 7. CDF of the 2D position errors for a phone carried in hand (see Fig. 5). Dashed lines are based on the synthetic 2D positions generated for each trajectory in Fig 5. Solid lines are based on the positions obtained by the fusion algorithm of the corresponding trajectory. The dashed blue line contains the best results, with ca. 95% of positions falling within 0.25 m error. The corresponding fused solution is less accurate with ca. 60% below 0.25 m error. For very noisy measurements (green), the advantage of the fused solution becomes clear, with ca. 78% of position errors below 0.74 m, versus ca. 0.47% for US* positions only.

the stand-alone PDR algorithm in orange, and the results of the fused method in green. Similar to the previous experiments, the trajectories based on PDR alone show the correct walking pattern, but with increasing deviation from the ground truth. These trajectories are not affected by the UIPS data and therefore not corrected after initialization.

For a phone carried in hand, the microphone is exposed directly to its surroundings, which increases its receptiveness to ultrasonic signals. Therefore, a hand-carried phone

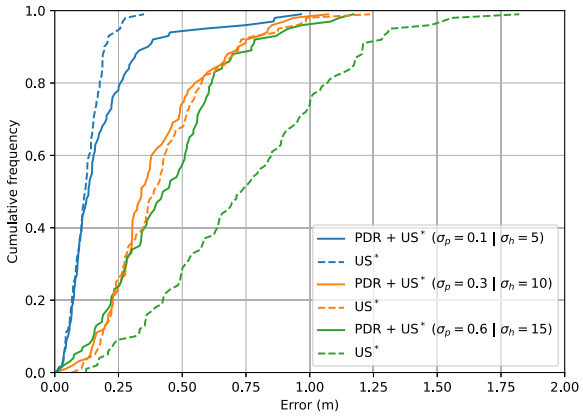

Fig. 8. CDF of the 2D position errors for a phone carried in the pocket (see Fig. 6). Dashed lines represent the errors of the synthetic 2D positions generated per trajectory. The synthetic positions are based on the same Gaussian noise as was used for a phone in hand (Fig. 7), and thus follow a similar trend. The solid lines represent the position errors produced by the fusion algorithm. These results are generally better than those obtained for a phone in hand, implying that the PDR algorithm is more robust for a phone in the pocket.

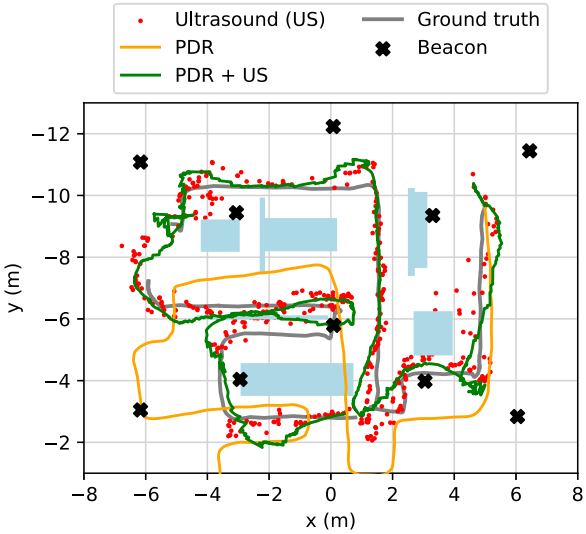

Fig. 9. Phone carried in hand, 10-beacon UIPS at 10 Hz. Red dots indicate US position measurements. Walking trajectory based on PDR is given in orange, and the results of the fused method is represented by the green line. The ground truth reference is given by the grey line.

is expected to produce high-accuracy ultrasonic position estimates. This is demonstrated by the small spread of red markers in Fig. 9, with most points falling within 0.75 m of the reference line. The position measurements become more noisy for a phone carried in the pocket, as shown by the red dots in Fig. 10. This is primarily due to the user blocking the direct line-of-sight between some of the beacons and the smartphone, as well as increased attenuation of the ultrasonic signal by clothing. This effect is clearly seen on the right side in Fig. 10.

For both phone positions, the fusion algorithm produces a continuous trajectory which follows a similar path as described by the individual UIPS position measurements, but smoother and less affected by outliers. As expected, the fused solution provides continuous tracking in areas with few ultrasound

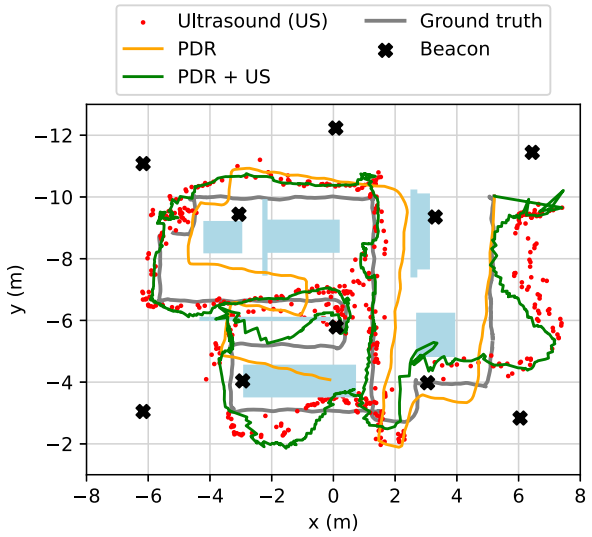

Fig. 10. Phone carried in the pocket, 10-beacon UIPS at 10 Hz. Ultrasonic positions are represented by red dots, the PDR-based trajectory in orange, and the fused PDR/US trajectory in green. Ground truth reference is shown in grey.

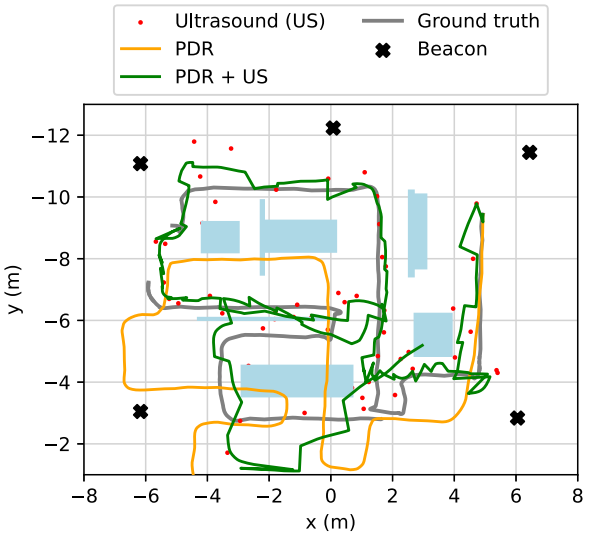

Fig. 12. Phone carried in hand, 5-beacon UIPS at 1 Hz. Red dots indicate US position measurements. Walking trajectory based on PDR is given in orange, and the fused method combining PDR and US data in green. The ground truth reference is given by the grey line.

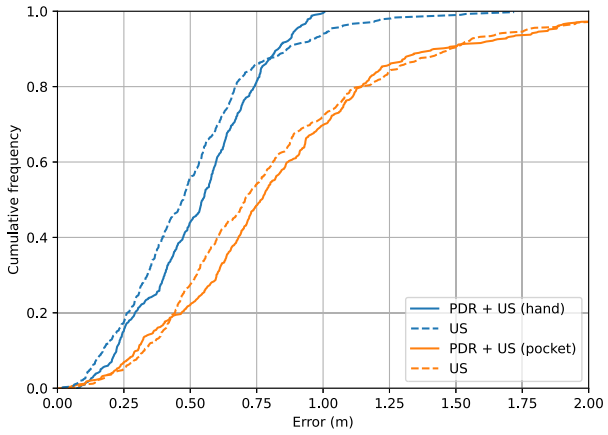

Fig. 11. CDF of the 2D position errors obtained from PDR and a 10-beacon UIPS at an update rate of 10 Hz (see Fig. 9 and 10). Results for a phone carried in hand are shown in blue, and for a phone carried in pocket in orange. Dashed lines represent the errors of the 2D positions obtained by the UIPS, whereas the solid lines represent the positions obtained by the fusion algorithm at the same time instances.

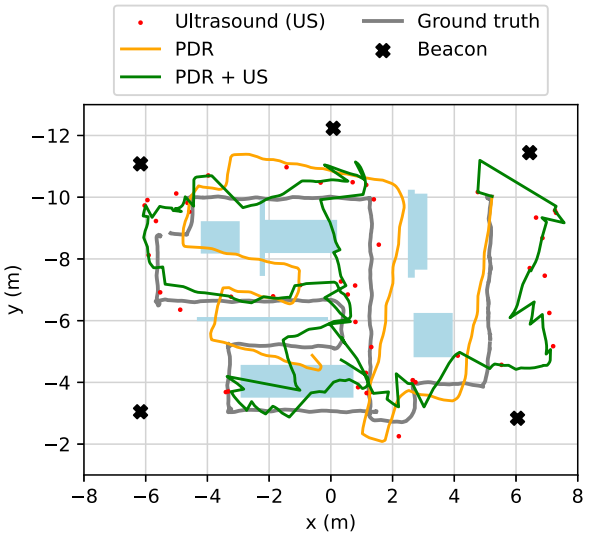

Fig. 13. Phone carried in pocket, 5-beacon UIPS at 1 Hz. Ultrasonic positions are represented by red dots, the PDR-based trajectory in orange, and the fused PDR/US trajectory in green. Ground truth reference is shown in grey.

measurements (such as the bottom-left part of both trajectories), and the ultrasonic updates mitigate drift and improve performance in areas of good coverage (center part). The fusion algorithm does not perform well, however, for areas of continuous measurement offset, such as shown on the right side in Fig. 10. Since this group of measurements contains a consistent offset towards the right, the fused solution also diverts towards that direction. It takes some time before the fusion-based trajectory corrects for this unwanted deviation. In contrast, trajectories based purely on interpolation between UIPS measurements are less affected by this, since each measurement is obtained independently.

The CDFs of the 2D position errors are shown in Fig. 11 for both phone positions. Based on the previous experiments with synthetic measurements, and the ultrasonic position errors found here, we would expect the fused solutions to produce better results than the UIPS by itself. This, however, is not reflected in the CDF plots, where adding PDR even seems to have a slight negative effect on the overall accuracy. As mentioned in the previous experiments, this may be due to limitations of PDR, rather than the fusion process itself. Another reason may be local areas of consistent measurement offset, as described above, as opposed to the Gaussian nature of the errors applied to the synthetic positions. Finally, the observed deviations may be due to incorrect estimation of the "measurement error" provided by the UIPS. Since these errors form the weights in the correction step of the Kalman filter, they have a direct effect on the accuracy of the fusion-based trajectory. While these factors seemingly reduce the

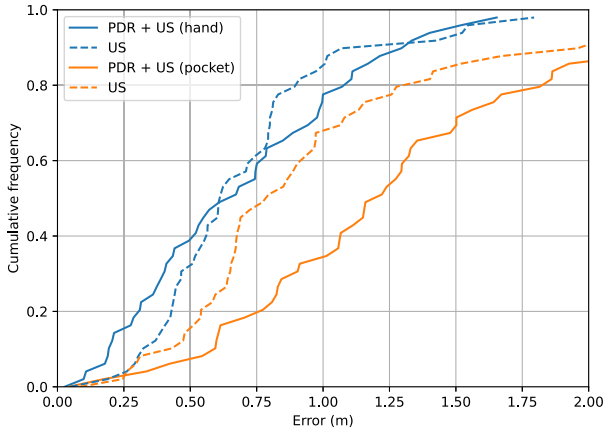

Fig. 14. CDF of the 2D position errors obtained from PDR and a 5-beacon UIPS at an update rate of 1 Hz (see Fig. 12 and 13). Phone carried in hand is shown in blue, and in orange a phone carried in the pocket. Dashed lines represent the 2D positions obtained by the UIPS, whereas the solid lines represent the positions obtained by the fusion algorithm at similar time intervals.

advantages of the fusion solution, adding PDR still mitigates the effect of large outliers and provides a smoother, continuous trajectory.

The previous experiments use a relatively high beacon density and update frequency. To simulate a more conservative situation, we repeated the same two experiments for a 5-beacon configuration and a reduced update rate of 1 Hz by subsampling at 1 second intervals. The results are shown in Fig. 12 for a phone in hand and Fig. 13 for a phone in pocket. The corresponding CDF plots of the 2D position errors are shown in Fig. 14. Since there are fewer measurements, a single measurement has a much stronger effect on the overall trajectory produced by the fusion algorithm. Still, the fusion-based trajectory is closer to ground truth, particularly for a phone in hand, than the trajectory based on PDR alone. Since the update frequency was reduced to 1 Hz, the UIPS system has a latency of up to one second, whereas the fused solution provides continuous position updates.

VI. Conclusion

This work introduces a novel step detection algorithm based on sine-wave approximation. The proposed method provides continuous and real-time step count information in the form of step fractions. Combined with inertial heading estimation, the proposed method yields a stand-alone PDR model. The PDR model is fused with a UIPS to account for error accumulation. The fused model, based on an EKF, provides a smoothed 2D trajectory for navigation applications for smartphone users.

We conducted multiple experiments in an open office setup with an area of approximately 150 m^2. The setup included furniture and panels to create a realistic scenario with NLOS conditions. Each experiment was performed for a phone carried in hand and a phone carried in pocket. First, we tested the accuracy of the step detection algorithm by walking along a trajectory of approximately 50 steps. This gave an accuracy of 97.5% for a phone in hand and 99.9% for a phone in pocket. Next, we validated the fusion algorithm by combining simulated and real PDR data with synthetic position and heading measurements at different noise levels. These experiments clearly demonstrate the feasibility of the PDR model and added value of the fused solution. Finally, we tested the fusion algorithm with a real UIPS. In this case, the furniture and walls created consistent offsets in the ultrasonic measurements, which introduced a strong deviation in some parts of the trajectory for the fused solution. Nevertheless, the system was able to recover after a series of accurate ultrasonic measurements were received, while providing a continuous and smoother trajectory than the US system by itself.

References

[1] R. Faragher and R. Harle, "Location fingerprinting with Bluetooth low energy beacons," *IEEE J. Sel. Areas Commun.*, vol. 33, no. 11, pp. 2418–2428, Nov. 2015.
[2] G. Chen, X. Meng, Y. Wang, Y. Zhang, P. Tian, and H. Yang, "Integrated WiFi/PDR/smartphone using an unscented Kalman filter algorithm for 3D indoor localization," *Sensors*, vol. 15, no. 9, pp. 24595–24614, 2015.
[3] G. M. Mendoza-Silva, J. Torres-Sospedra, and J. Huerta, "A meta-review of indoor positioning systems," *Sensors*, vol. 19, no. 20, pp. 1–45, 2019.
[4] J. Aparicio, T. Aguilera, and F. J. Álvarez, "Robust airborne ultrasonic positioning of moving targets in weak signal coverage areas," *IEEE Sensors J.*, vol. 20, no. 21, pp. 13119–13130, Nov. 2020.
[5] J. A. Paredes, T. Aguilera, F. J. Álvarez, J. Lozano, and J. Morera, "Analysis of Doppler effect on the pulse compression of different codes emitted by an ultrasonic LPS," *Sensors*, vol. 11, no. 11, p. 10765–10784, 2011.
[6] R. R. Hobbs, *Marine Navigation 1: Piloting* (Fundamentals of Naval Science), 2nd ed. Annapolis, MD, USA: Naval Institute Press, 1981, ch. 8.
[7] Z. Berman and J. D. Powell, "The role of dead reckoning and inertial sensors in future general aviation navigation," in *Proc. IEEE PLANS*, Palm Springs, CA, USA, Apr. 1998, pp. 510–517.
[8] H. H. Hall, "Alternate approaches to automotive navigation," *SAE Trans.*, vol. 95, no. 4, pp. 514–520, 1986.
[9] W. Kang and Y. Han, "SmartPDR: Smartphone-based pedestrian dead reckoning for indoor localization," *IEEE Sensors J.*, vol. 15, no. 5, pp. 2906–2916, May 2015.
[10] Y. Wu, H.-B. Zhu, Q.-X. Du, and S.-M. Tang, "A survey of the research status of pedestrian dead reckoning systems based on inertial sensors," *Int. J. Autom. Comput.*, vol. 16, no. 1, pp. 65–83, 2019.
[11] H. Zhao, L. Zhang, S. Qiu, Z. Wang, N. Yang, and J. Xu, "Pedestrian dead reckoning using pocket-worn smartphone," *IEEE Access*, vol. 7, pp. 91063–91073, 2019.
[12] X. Hou and J. Bergmann, "Pedestrian dead reckoning with wearable sensors: A systematic review," *IEEE Sensors J.*, vol. 21, no. 1, pp. 143–152, Jan. 2021.
[13] S. Park, J. H. Lee, and C. G. Park, "Robust pedestrian dead reckoning for multiple poses in smartphones," *IEEE Access*, vol. 9, pp. 54498–54508, 2021.
[14] Z. A. Deng, G. Wang, D. Qin, Z. Na, Y. Cui, and J. Chen, "Continuous indoor positioning fusing WiFi, smartphone sensors and landmarks," *Sensors*, vol. 16, no. 9, p. 1427, Sep. 2016.
[15] H.-H. Lee, S. Choi, and M.-J. Lee, "Step detection robust against the dynamics of smartphones," *Sensors*, vol. 15, no. 10, pp. 27230–27250, 2015.
[16] Y. Cho, H. Cho, and C.-M. Kyung, "Design and implementation of practical step detection algorithm for wrist-worn devices," *IEEE Sensors J.*, vol. 16, no. 21, pp. 7720–7730, Nov. 2016.
[17] M. Zhang, Y. Wen, J. Chen, X. Yang, R. Gao, and H. Zhao, "Pedestrian dead-reckoning indoor localization based on OS-ELM," *IEEE Access*, vol. 6, pp. 6116–6129, 2018.
[18] M. Basso, M. Galanti, G. Innocenti, and D. Miceli, "Pedestrian dead reckoning based on frequency self-synchronization and body kinematics," *IEEE Sensors J.*, vol. 17, no. 2, pp. 534–545, Jan. 2017.
[19] X. Kang, B. Huang, and G. Qi, "A novel walking detection and step counting algorithm using unconstrained smartphones," *Sensors*, vol. 18, no. 1, pp. 1–15, 2018.
[20] Y. Yao, L. Pan, W. Fen, X. Xu, X. Liang, and X. Xu, "A robust step detection and stride length estimation for pedestrian dead reckoning using a smartphone," *IEEE Sensors J.*, vol. 20, no. 17, pp. 9685–9697, Sep. 2020.

[21] S. Y. Park, S. J. Heo, and C. G. Park, "Accelerometer-based smartphone step detection using machine learning technique," in *Proc. iEECON*, Mar. 2017, pp. 1–4.
[22] M. Susi, V. Renaudin, and G. Lachapelle, "Motion mode recognition and step detection algorithms for mobile phone users," *Sensors*, vol. 13, no. 2, pp. 1539–1562, Jan. 2013.
[23] V. Renaudin and C. Combettes, "Magnetic, acceleration fields and gyroscope quaternion (MAGYQ)-based attitude estimation with smartphone sensors for indoor pedestrian navigation," *Sensors*, vol. 14, no. 12, pp. 22864–22890, 2014.
[24] Z.-A. Deng, G. Wang, Y. Hu, and D. Wu, "Heading estimation for indoor pedestrian navigation using a smartphone in the pocket," *Sensors*, vol. 15, no. 9, pp. 21518–21536, 2015.
[25] A. Manos, I. Klein, and T. Hazan, "Gravity-based methods for heading computation in pedestrian dead reckoning," *Sensors*, vol. 19, no. 5, pp. 1–19, 2019.
[26] V. Thio, K. B. Ånonsen, and J. K. Bekkeng, "Relative heading estimation for pedestrians based on the gravity vector," *IEEE Sensors J.*, vol. 21, no. 6, pp. 8218–8225, Mar. 2021.
[27] S. J. Kim and B. K. Kim, "Dynamic ultrasonic hybrid localization system for indoor mobile robots," *IEEE Trans. Ind. Electron.*, vol. 60, no. 10, pp. 4562–4573, Oct. 2013.
[28] P. Lazik, N. Rajagopal, O. Shih, B. Sinopoli, and A. Rowe, "ALPS: A Bluetooth and ultrasound platform for mapping and localization," in *Proc. ACM SenSys*, New York, NY, USA, Nov. 2015, pp. 73–84.
[29] A. Ens *et al.*, "Acoustic self-calibrating system for indoor smart phone tracking," *Int. J. Navigat. Observ.*, vol. 2015, pp. 1–15, Feb. 2015.
[30] H. Yang *et al.*, "Smartphone-based indoor localization system using inertial sensor and acoustic transmitter/receiver," *IEEE Sensors J.*, vol. 16, no. 22, pp. 8051–8061, Nov. 2016.
[31] D. Gualda *et al.*, "LOCATE-US: Indoor positioning for mobile devices using encoded ultrasonic signals, inertial sensors and graph-matching," *Sensors*, vol. 21, no. 6, pp. 1–25, 2021.
[32] T. Ji and A. Pachi, "Frequency and velocity of people walking," *Struct. Eng.*, vol. 84, no. 3, pp. 36–40, 2005.
[33] V. Thio, J. Aparicio, K. B. Ånonsen, and J. K. Bekkeng, "Experimental evaluation of the Forkbeard ultrasonic indoor positioning system," *IEEE Trans. Instrum. Meas.*, Dec. 2021, doi: 10.1109/TIM.2021.3136261.
[34] *Forkbeard Technologies AS*. Accessed: Nov. 19, 2021. [Online]. Available: https://forkbeardtech.com/technology/

Vincent Thio (Member, IEEE) received the M.Sc. degree in geophysics from Utrecht University, The Netherlands, in 2015. He is currently pursuing the Ph.D. degree in physics with the University of Oslo, Norway. From 2016 to 2018, he worked as a Reservoir Engineer at Shell. His research interests include indoor localization and navigation, ultrasound-based positioning, and sensor fusion.

Joaquín Aparicio (Member, IEEE) received the degree in physics from the University of Extremadura, Badajoz, Spain, in 2008, and the Ph.D. degree in electronics from the University of Alcalá, Alcalá de Henares, Spain, in 2014. From 2015 to 2018, he was a Postdoctoral Researcher at the Japan Agency for Marine-Earth Science and Technology, Yokosuka, Japan. Since 2018, he has been a Postdoctoral Fellow with the Department of Informatics, University of Oslo, Oslo, Norway. His research interests include positioning systems, acoustic propagation, signal processing, and communication systems.

Kjetil Bergh Ånonsen received the M.Sc. degree in applied mathematics and the Ph.D. in engineering cybernetics from the Norwegian University of Science and Technology (NTNU). He is a Senior Scientist with the Navigation Group, Norwegian Defense Research Establishment (FFI). He joined FFI in 2007. Since 2018, he has also had a part-time position as an Adjunct Professor at the Department of Technology Systems, University of Oslo.

Jan Kenneth Bekkeng received the Ph.D. degree in physics from the University of Oslo, Norway, in 2007, on spacecraft attitude determination and instrumentation. He joined the Norwegian Defence Research Establishment (FFI) in 2007 and a Principal Scientist in 2016. He joined as a Researcher with the Department of Physics, University of Oslo, in 2007. He became an Associate Professor II in 2010. His current research interests include electronic warfare, infrared and electro-optical systems, missiles, modeling and simulation, estimation, navigation, and tracking. He is a member of technical teams in NATO, including NATO Science and Technology Organization (STO).

Wilfred Booij received the Ph.D. degree in physics from Cambridge University. Previously, he worked at Sonitor, Shell, and HP. He is currently the CTO at Forkbeard Technologies AS. He has over 15 years of management and engineering experience in the field of indoor positioning and holds close to 100 patents.